Journal of The Electrochemical Society, **154** (4) D249-D259 (2007)
0013-4651/2007/154(4)/D249/11/$20.00 © The Electrochemical Society

The Effect of rf-Irradiation on Electrochemical Deposition and Its Stabilization by Nanoparticle Doping

Yael Katsir,[a] Lior Miller,[b] Yakir Aharonov,[a] and Eshel Ben Jacob[a,z]

[a] *School of Physics and Astronomy, Raymond and Beverly Sackler Faculty of Exact Sciences, The Maguy-Glass Chair in Physics of Complex Systems, Tel Aviv University, 69978 Tel Aviv, Israel*
[b] *Department of Materials Engineering, Technion—Israel Institute of Technology, Haifa 32000 Israel*

Qualitative observations of electrochemical deposition in thin circular cells have shown that radio-frequency (rf) irradiation of zinc sulfate solutions can dramatically affect the deposition patterns. For some growth parameters the rf-treatment can even induce morphology transitions between the dense branching morphology and dendritic growth. We found that the effects of rf-treatments can last for a long time (hours). In addition, detailed studies using electron microscopy observations reveal that the effects span on all scales, from the micrometer-scale organization to the self-organization of the macroscopic pattern. We propose that these changes of patterning on all scales resulted from singular effects of gas-filled submicrometer bubbles or nanobubbles, which are generated by the rf-irradiation. The idea is that hydration shells around the nanobubbles induce water ordering that acts as a new singular perturbation mechanism in the solution. The latter is in addition to the well studied microscale singular perturbation mechanisms in the deposit (surface tension and attachment kinetics). We also studied electrochemical deposition in zinc sulfate solutions prepared from water that is doped with nanoparticles under rf-irradiation, and found similar and even amplified effects. Moreover, the nanoparticle doping stabilizes the effects—they are retained months after the solutions were prepared.
[DOI: 10.1149/1.2437055]

Manuscript submitted September 18, 2006; revised manuscript received December 6, 2006.
Available electronically February 20, 2007.

Electrochemical deposition (ECD) of metals in thin gap geometry has been widely used over the last twenty years to study the foundation of pattern formation and self-organization in open systems far from equilibrium.[1-41] First, a great variety of macroscopic patterns (morphologies) are formed as a function of several control parameters: applied voltage, initial concentration, chemical composition of the solutions, its viscosity etc. Second, it is relatively straight forward to perform both qualitative and quantitative measurements of the formed morphologies as well as the dynamics in the surrounding fluid. For example one can study the correspondence between structure and the response current (or the response voltage),[33,39,41] as well as between the structure and the concentration field[20] and convection patterns in the solution.[27-29] Third, and perhaps most important, it is possible to measure directly the patterning on all scales from the crystalline structure on the microscopic scale [using X-ray and transmission electron microscopy (TEM) measurements], through the nano and micrometer scales organization [using TEM and scanning electron microscopy (SEM) measurements] to the macroscale patterning.[5,7,10-16,35,37,38] Such measurements on all scales played a crucial role in establishing the theoretical framework about the micro-macro singular interplay reflected in the morphology selection and morphology transitions.[10-14,22,42-50] In particular, electron microscopy studies of the deposition morphologies in thin circular cells showed that the dendritic morphologies are characterized by ordered patterns down to the micrometer scale with crystalline structure while the dense branching morphologies (DBM) are not ordered and have polycrystalline or amorphous structures at the microscopic level resulted in rings in the diffraction pattern..[5,10-14,38]

It is now understood that the pattern formation results from a competition between the macroscale diffusive instability (connected with the ion transport in the solution) which drives the patterns towards decorated, irregular, scale free shapes, and the microscopic-scale dynamics at the interface (connected with surface tension, attachment kinetics, and crystalline anisotropy), which imposes local characteristic length scales and overall symmetries.[10-14,42-50] Out of equilibrium (i.e., finite voltage), the transport processes are intensified and at the same time they amplify the microscopic dynamics. As a result the microscopic dynamics act as a singular perturbation that can reach up and affect the macrolevel organization (we note that the mathematical term singular perturbation describes the situation in which very small change in the equation causes a new solution).[10-14,42-54] By the same token, the global tendency, acting as singular feedback, can reach down and affect the microlevel organization by favoring one particular small-scale structure over the others.[10-13]

Thus, according to the new theoretical framework, the balance in the competition is determined via singular interplay between the micro- and macrolevels. The two-level picture is often insufficient.[10-13] In such cases, a hierarchic multilevel organization is the only solution to fulfill the imposed self-consistency (solvability) requirement. We now know that beside surface tension, attachment kinetics, and crystalline anisotropy, other effects can act as singular perturbation that completely alter the growth patterns, e.g., impurities in solidification from supersaturated solution turn the dendritic pattern into needlelike crystal shapes.[55]

In the context of electrochemical deposition it has been shown that induced convection,[29] changes in the solution viscosity,[36] mixing of different cations,[10] and organic molecule additives[56,57] can all act as singular perturbations.

The preliminary studies presented in Ref. 14 showed that radio-frequency (rf)-irradiation (in the MHz frequency range) of zinc sulfate solutions (prior to deposition) can induce morphology transitions between the DBM and dendritic growth. The studies presented here are aimed at better understanding this interesting phenomenon. For that we performed detailed studies of the effects of rf-irradiation (in the MHz frequency range) on ECD in thin circular cells and focused on comparison between the deposition structures of growth in rf-treated and in nontreated solutions. We found that in addition to the induced morphology transitions reported in,[14] the rf-treatment can also induce significant changes in the structure of the DBM and dendritic morphologies. Using electron microscopy observations we found that the effects span on all scales, from the microscopic structure through the micrometer-scale organization to the macroscopic pattern. Following Ref. 58, our guiding assumption is that the effects of rf-irradiation are mainly mediated via the formation of stable nanobubbles in the solution. In the next section we provide a concise summary of previous studies that support the idea that rf-irradiation of water can lead to the formation of stable (hours) array of gas nanobubbles[59,60,65,67] A new idea hinted at by the experimental findings presented here is that the ordered shell of the nanobubbles induces long range water structure and that this induced order can act as new singular perturbation mechanisms that affect patterning both on the micro- and macrolevels.

We also studied electrochemical deposition in solutions made

---

[z] E-mail: eshel@tamar.tau.ac.il

from rf-irradiated water that is doped with nanoparticles (barium titanate, $BaTiO_3$) that are injected during the rf-treatment (see the Appendix for details). We found similar and even more pronounced effects in the solutions made from the nanoparticles doped water (NPD water) to those in the rf-irradiation of zinc sulfate solution made from RO (reverse osmosis) distilled water. Moreover, the nanoparticle doping generates durable stabilization of the effects—they are retained months after the solutions were prepared. To explain the observations we propose that the doping process might stabilize the nanobubbles and/or the nanoparticles also surrounded by a shell of ordered water molecules similar to the clathrate shell of the nanobubbles.

The Effects of rf-Irradiation on Water and Aqueous Solutions

During the past two decades, much effort has been devoted in various fields of science and engineering to study the effects of rf-irradiation on the behavior of aqueous solutions and suspensions.[58-75] The following long term effects of rf treatment are currently well documented. (1) Intake of dissolved air from the water into nanobubbles and formation of nanobubbles.[59,60,67,70] (2) A decrease in surface tension from 72 to 68 dyn/cm.[66] (3) Increase in the intensity of all three infrared (IR) spectroscopy frequency bands: 3200 cm^{-1} (strong hydrogen bonds), 3400 cm^{-1} (distorted hydrogen bonds), and 3600 or 3750 cm^{-1} (nonbonded molecules) by about 30%.[67] (4) Increase in the concentration of atomic hydrogen.[66] The presence of the atomic hydrogen lasted for months and has been stable with respect to boiling as well as freezing the water. (5) Modifications in the spectra of dissolved hydrophobic fluorescent molecules (but not the spectra of hydrophilic ones).[68] (6) The zeta potentials of rf treated suspensions and solutions show oscillations with about a 25 min period that can last for hours after treatment.[63,64] (7) Enhancement of cement hydration.[81] (8) Fesenko and co-workers found significant changes in the opening frequency of potassium channels in cells that are grown in solutions that were treated by rf signals.[82-84] (8) Ben Jacob and co-workers found an increase in the growth rate of bacteria grown in aqueous solutions that were treated by rf signals.[14,58]

These phenomena pointout that rf-treatments of water and aqueous solutions induce physical alterations in the water structure that can last for hours after treatment (dubbed "water memory"). It was proposed that the long term stability of water structure resulted from the formation of a dense array of stable gas nanobubbles in the water.[58-60,67] The crucial role of gas nanobubbles is evident from the observations that rf-treatment does not have an effect on water that was outgassed before the treatment and outgassing of rf-treated water and solutions erases all the effects. It is also important to keep in mind that much of the interaction of the rf signals is with gas/liquid interfaces of the nanobubbles.[67]

Still, the idea of stable nanobubbles was discarded based on two strong arguments. (1) The nanobubbles are expected to dissolve rapidly due to the high Laplace pressure (the internal pressure due to the interfacial curvature). (2) The claimed anomalous effects of rf-irradiation could not be explained based on the current commonly accepted theories of water.[85-92] It was agreed that accepting the anomalous effects as being real (and not a reflection of overlooked artifacts) poses a challenging problem in modern physical chemistry. Therefore, these unusual effects were in general regarded until recently as rather anecdotal phenomena. Things begun to change less than a decade ago when advanced methods were used to quantify the above mentioned effects of rf-irradiation. And, more recently, following the direct observations of nanobubbles [using liquid atomic force microscopy (AFM) in high resolution tapping mode] on hydrophobic surfaces revealed that, once formed, the nanobubbles can be stable for hours.[76-80] To summarize, according to the new nanobubbles-based paradigm the following is proposed. (1) The nanobubbles have long term stability (hours). This assumption is supported by direct observations using AFM.[76-80] (2) The gas-water interface of the nanobubbles is hydrophobic and therefore at the interface the water molecules form clathrate shells with an "icelike" structure. This assumption is supported almost directly by measured changes in IR spectroscopy.[67] (3) The ordered shells induce order in the water molecules surrounding the nanobubbles that can extend up to a micrometer in range. This idea is indirectly supported, for example, by the effect on zeta potential[68] and the fluorescence of hydrophobic molecules.[63,64] We note that ordered water should be effectively less hydrophilic since it is expected that the entropy of mixing of hydrophilic molecules will be lower than that of mixing in the absence of order.

According to the new paradigm the original objections to the idea of stable nanobubbles are based on macroscale consideration that does not take into account the special properties of the air-water interface and the existence of the ordered clathrate shells caging the nanobubbles. Hence it is argued that entropy contributions can provide possible, yet to be discovered, stabilization mechanisms of the nanobubbles and should be included in the theory.[67,69,70,75,88] Inspired by the similarity in the effects on the zeta potential that have been observed for colloidal particles and gas nanobubbles, it was suggested that ions from the solution are integrated in the nanobubbles shell and provide extra stabilization. Others call for considerations beyond the classical theory of water (that is based on the water molecule as an electric and magnetic dipole), and suggest that effects related to the quantum mechanics differences between the two nuclear spin isomers, ortho- and para water, participate in the stabilization of the nanobubbles. We take the view that these mechanisms are not mutually exclusive and probably both relevant. More specifically, we follow the idea that since the nanoscale is outside the thermodynamic limit, the standard statistical physics considerations should be modified and that nonlinear and even collective quantum effects might play a significant role.

Keeping in mind that the induced order around each of the nanobubbles can extend over a distance larger than that between the bubbles, it is reasonable to assume that the induced order mediates bubble-bubble interactions. In the conclusions, we propose that these exchange interactions have a singular collective effect: The bubbles self-organize to form a pliable network with hierarchical organization (clusters of small bubbles around larger ones and clusters of clusters). We expect that the formation of such a network can afford elevated stability and hence is consistent with the observed long decay time of the rf-treatment effects. The idea is that there is an exchange of gas molecules from the smaller nanobubbles to the larger ones (due to the imbalance in the internal Laplace pressure). In the absence of bubble-bubble interactions, this process causes the large bubbles to expand and float to the surface after exceeding a critical radius due to Archimedes force. We propose that due to bubble-bubble interactions, the smaller bubbles surround the larger ones (that serve as the hubs of the clusters) and hold them against the Archimedes force so the critical radius for detachment is much larger. In addition, we propose that the formation of the ordered shell together with the water around the nanobubbles being less hydrophilic should slow the rate of gas exit from the bubbles.

Experimental

The experiments reported here were performed in quasi-two-dimentional electrochemical cells with a circular geometry. The electrolyte (zinc sulfate) solution is held between two Perspex plates with 0.3 mm spacing. The ECD cell consists of a central copper plate cathode, of diameter 30 mm and thickness 0.3 mm, and a circumferential copper wire (0.5 mm thick) anode that forms a circle with 93.5 mm diameter. Zinc sulfate solutions are usually prepared from reverse osmotic (RO) water using commercial zinc sulfate ($ZnSO_4 \cdot 7H_2O$, Sigma-Aldrich). Copper electrodes were used to ease the construction of the cell. We note that the growth is not affected by the use of copper electrodes as long as the deposit does not get closer than 1 cm from the anode. At shorter distances cooper ions that are dissolved from the anode integrate within the deposit and change both the microscopic and macroscopic patterns.[10] In the experiments presented here we compared the growth patterns (the

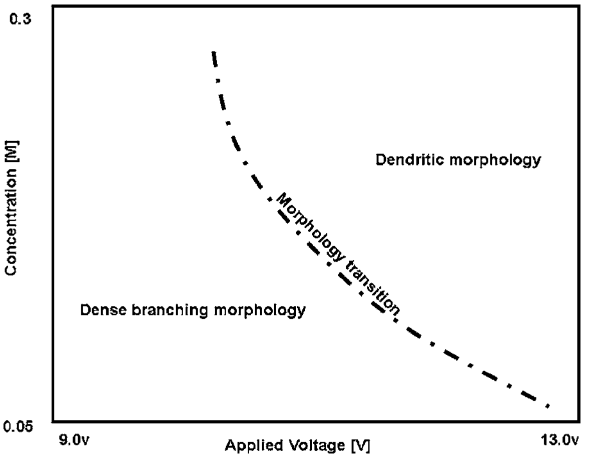

Figure 1. A schematic representation of the concentration versus voltage (CV) morphology diagram for the ECD cells used in this study.

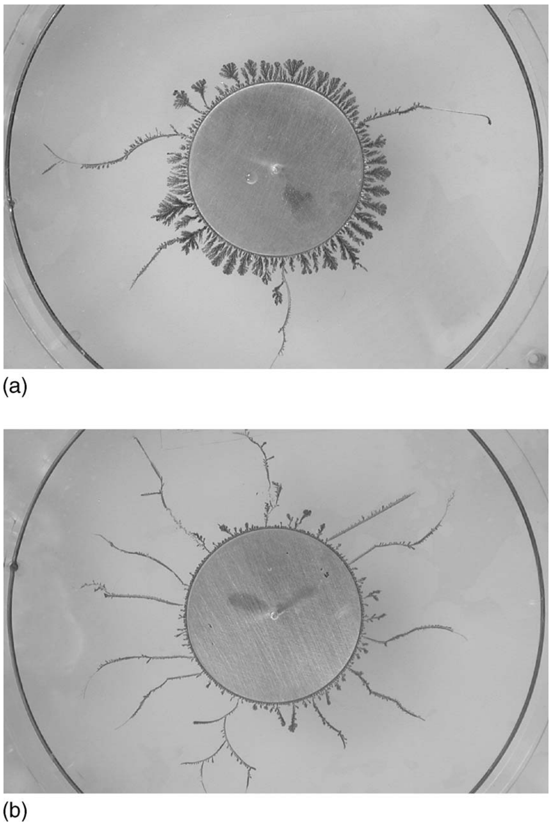
(a)

(b)

Figure 2. The macroscale patterning of (a) a typical DBM and (b) a dendritic morphology. Growth conditions in (a) are $C = 0.2$ M and $V = 11.0$ V and in (b) are $C = 0.3$ M and $V = 13.0$ V.

morphology transitions) when the deposits were more than 1 cm away from the anode. Hence we do not expect the process to be affected by the dissolved copper ions.

The ECD process was performed under constant voltage conditions while monitoring the response current. The voltage (cell potential) is applied 10 min after placing the solution and closing the cell. The deposition time was changed with the concentration and the applied voltage, and it was typically 8–10 min for the DBM and 5–7 min for the dendritic morphology.

For the electron microscopy characterization we cooled the cells at the end of the deposition (while the applied voltage is on) using liquid nitrogen for fast freezing and then the deposits were dried in a vacuum desiccator and kept until they were inserted into the microscope chamber (ultrahigh vacuum). This procedure was used to reduce equilibration and oxidation processes at the deposited surfaces before characterization.[10] To do so we used disposable cells. Hence, although the results are qualitatively reproducible, one has to keep in mind that there are some quantitative variations from cell to cell. Quantitative variations also resulted from the RO water and the NPD-water used for preparing the solutions. We monitored the conductivity of the solutions before deposition and found that it is about 18.9×10^{-3} Siemens with about $\pm 0.15 \times 10^{-3}$ Siemens variations for all cases (i.e., for the solutions made from the RO water and the NPD-water as well as after the rf-treatment of the solutions made from the RO water). The presented results are the typical ones. To test the generality of the effect we also used solutions made from MOS and HPLC water.

Morphology Diagram

In Fig. 1 we present a schematic concentration-voltage (CV) morphology diagram of the deposition process in the cells used in our experiments. Since we focus on the morphology transition between the DBM and the dendritic morphology we map a window of $0.05 \text{ M} < C < 0.3 \text{ M}$ and $9.0 \text{ V} < V < 13 \text{ V}$. Similar to the findings of Grier et al.,[5] the morphology transition is from DBM at lower voltages (cell potentials) to dendritic growth at the higher voltages. Also, in agreement, the transition voltage is higher for lower concentrations. Several of the comparative studies were performed for $C = 0.2$ M and $V = 12.4$ V that is on the dendritic side of the morphology diagram but close to the morphology transition voltage.

Illustration of the macroscopic patterns of the DBM and the dendritic morphologies during ECD (similar to the results presented, for example, in Ref. 5 and 10-13) is presented in Fig. 2. Figure 2a corresponds to the DBM and Fig. 2b to the dendritic growth. Electron microscopy observations reveal that the differences between the macroscale patterns of the different morphologies go hand in hand with different organization on the microscopic scale[5,10-12] as is shown later. We found that close to the morphology transition, the branches of the DBM are composed of short dendrites with random orientations. At lower voltages and lower concentrations the branches are composed of small crystals with random orientations. The different morphologies are also characterized by the functional dependence of the response current during the deposition (the current-time characteristics) as presented in Fig. 3.

The Macrolevel Effect of rf-Irradiation

The effect of the rf-treatment on the macroscopic scale is most pronounced at the vicinity of the morphology transition. Hence we mainly focused on macrolevel comparison of the ECD patterning between control and rf-irradiated solutions for $C = 0.2$ M and $V = 12.4$ V. For the rf-treatment we used electromagnetic signals with a narrow band located at a frequency of 915 MHz and broadcast through a linear antenna that is immersed in a water tank at 25 °C. We irradiated 50 mL of zinc sulfate solution in a glass bottle that is placed adjacent to the antenna in the same water tank.

In Fig. 4 we demonstrate that for these conditions a DBM pattern emerges in the rf-treated solution instead of the dendritic growth in the case of the untreated solution. We also demonstrate that the effect of the rf-treatment lasts for over an hour. We note that the results presented here reproduce those reported in.[14] Different protocols of rf-treatment lead to the same effect of DBM growth instead of the dendritic one but the DBM pattern is somewhat different for each case as illustrated in Fig. 4 and 5.

From a pattern formation perspective we note that in the context of Saffman-Taylor fingers (formed while air is pushed into a viscose fluid[10]) it has been shown that a small air bubble (about millimeter size) placed at the tip of the finger can provide stabilization against the tip-splitting instability. Consequently, instead of the ordinary tip-

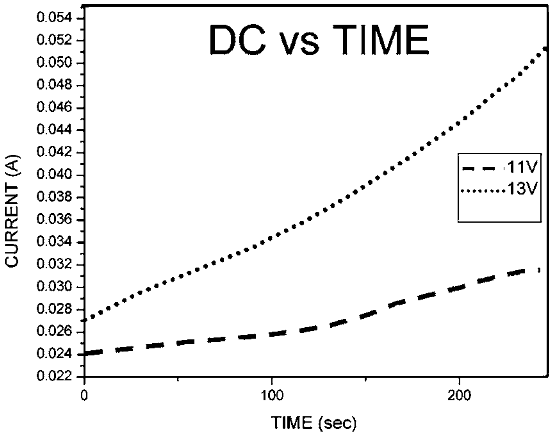

Figure 3. Comparison between the time dependence of the response current for the DBM (at $C = 0.2$ M and $V = 11$ V) (the dashed curve) and the dendritic growth (at $C = 0.3$ M and $V = 13$ V) (the dotted curve). Note the differences in the functional dependence of the current for the two morphologies. This behavior is connected with the selection of the growing morphology. According to the fastest growing morphology selection principle, the faster morphology is the selected one as explained in Ref. 10-13 and 42-50.

splitting pattern, the finger forms a dendrite (parabolic shaped tip and emergence of side branches[93-95]). This phenomenon might lead one to expect that the formation of nanobubbles by the rf-treatment should lead to the selection of dendritic growth rather than the DBM one. The fact that we observed the opposite effect provides additional support to the idea (presented in the Introduction) that the nanobubbles form a network that induces long-range water ordering for the following reasons: As was mentioned in the Introduction a microlevel singular perturbation mechanism that involves symmetry breaking is required for dendritic growth. In solidification it is known that the crystal structure of the solid leads to anisotropic surface tension and anisotropic kinetic of attachment that act as the singular perturbation mechanisms that lead to dendritic growth. In penetration of air into viscous fluid there is no internal anisotropy. Hence an external singular symmetry breaking perturbation is needed for dendritic growth as was demonstrated by Ben Jacob et al.[10-13,51] These results and the effect of a bubble placed at the tip of the air finger demonstrate that an external mechanism can also act as a singular perturbation during pattern formation. Electrochemical deposition is similar to solidification as the crystalline structure of the metal deposit provides internal singular perturbation that can lead to dendritic growth in the absence of externally induced ordering. In the specific case of zinc deposition the anisotropy is so large that at high voltages the DBM is composed of relatively short dendrites with random orientation as will be presented later. This phenomenon probably emerged as a result of competition between the internal anisotropy and variations due to convective dynamics around the deposit.[33] We propose that in the case of rf-treated solutions, the long range water structure generated by the nanobubbles has its own ordering that competes with the internal anisotropy of the growing deposit and hence selects the DBM. This idea is supported by the microscopic observations of the deposits as will be shown further on.

The Macrolevel Effect of Nanoparticle Doping (NPD)

In this section we proceed to show results on the macrolevel patterning of electrochemical deposition in zinc sulfate solutions prepared from nanoparticles doped water (NPD-water)—water that is doped with nanoparticles (barium titanate $BaTiO_3$) under rf-irradiation. A more detailed description of the production process and the physical characterization of this NPD-water are presented in the Appendix (the Neowater™ by Do-Coop Technologies Ltd.).

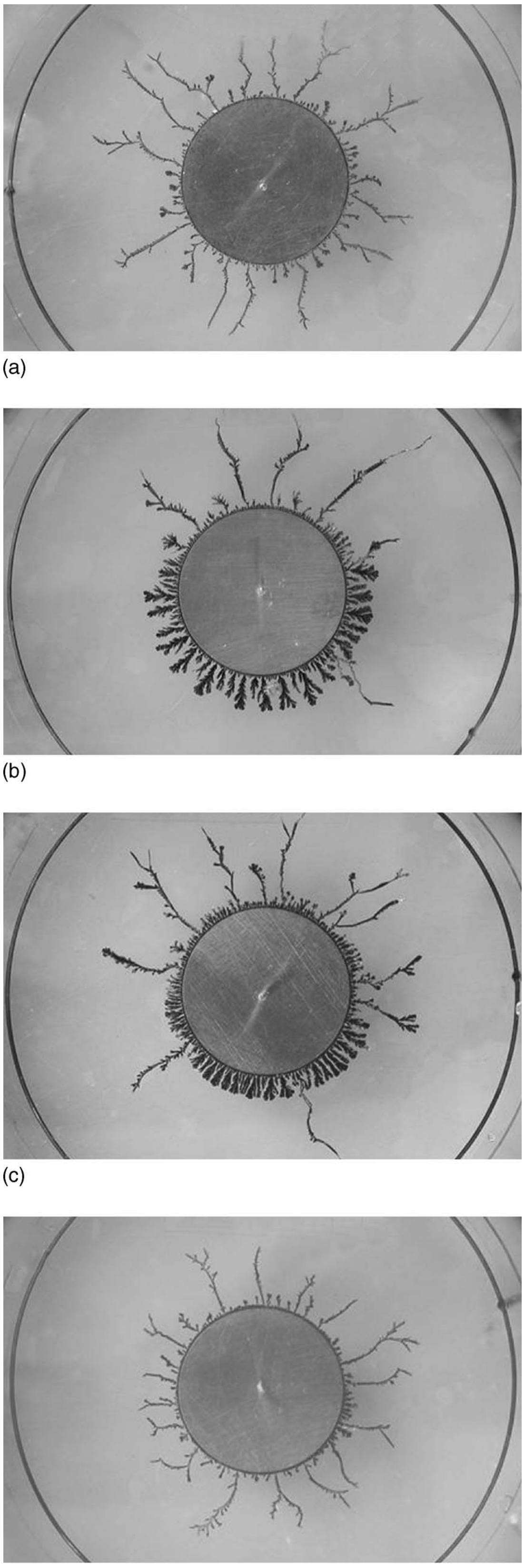

Figure 4. Induced morphology transition. (a) The emerged morphology for the control deposition for $C = 0.2$ M and $V = 12.4$ V. (b) The emerged morphology in the rf-irradiated solution 20 min after treatment. (c) The emerged morphology after 40 min. (d) The emerged morphology after 96 min. The rf signal was applied at power $P = 15$ W and frequency 915 MHz for 30 min.

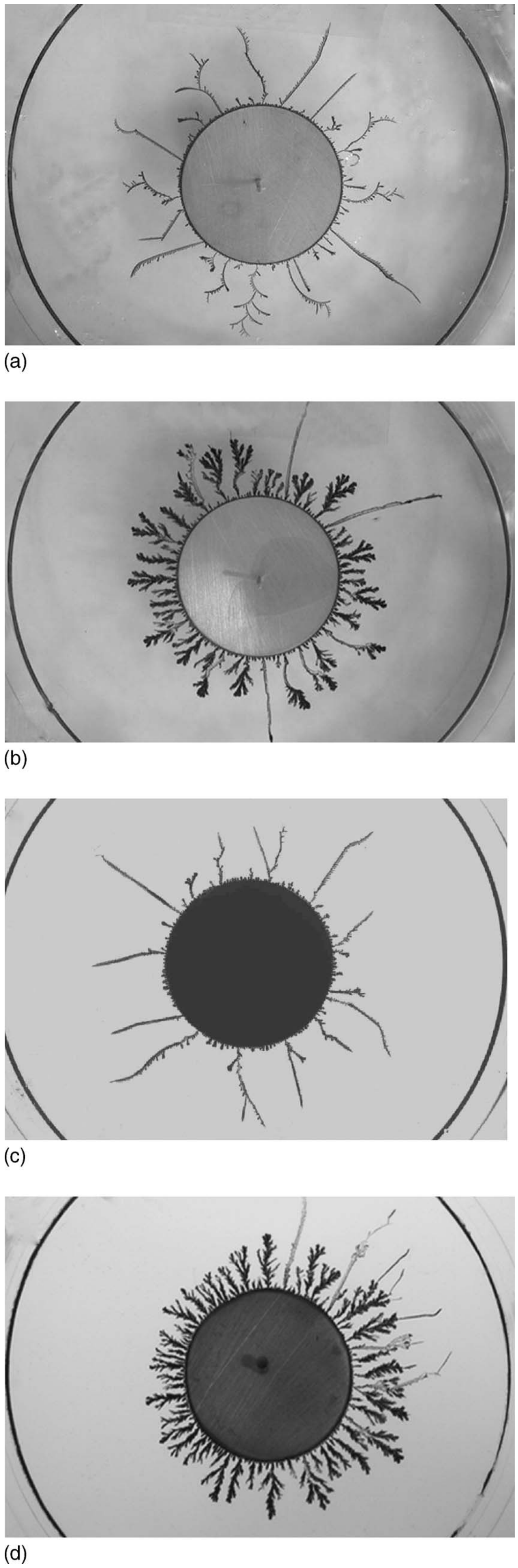

Figure 5. The effect of (b) the rf-treatment vs (a) control using power of $P = 15$ W and frequency 915 MHz for 30 min. The deposition started 45 minutes after the rf-treatment. The results of Ref. 14 are shown in (c) and (d) for control and rf-irradiated solution, respectively. The rf-treatment was at 915 MHz using power of $P = 15$ W for 17 min and the deposition started 30 min after the rf-treatment.

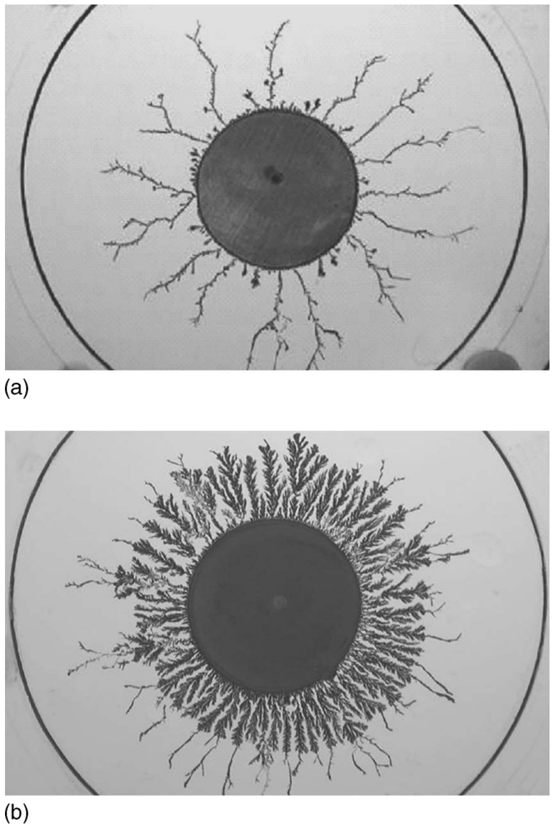

Figure 6. The effect of nanoparticle doping on (b) the electrochemical deposition vs (a) control for $V = 12.4$ V and $C = 0.2$ M. In these experiments MOS water was used both for the control and the preparation of the doped water.

In Fig. 6 we show that similar to the case of the rf-treatment the nanoparticle doping leads to the selection of the DBM pattern over the dendritic one at $C = 0.2$ M and $V = 12.4$ V. More specifically, for growth conditions at which dendritic growth is observed for control solutions (made from RO or MOS water), DBM patterns emerge for ECD in solutions made from the NPD-water. We notice that the effect is more pronounced in comparison to that of the rf-treatment in the sense that the DBM pattern is denser and the transition to the dendritic growth starts at a larger radius, i.e., at later times.

As described in the Appendix, the NPD-water contains some residual level of Ba^+ cations. From previous studies it is known that mixing of different cations can act as a singular perturbation that changes the growth pattern.[10] Therefore, in principle, the observed effect can resulted from the free barium cations. So, we performed ECD experiments and found that a detectable effect is indeed observed for concentrations down to about 10^{-3} to 10^{-2} M. Since the concentration of the barium cations is lower than 1 μM, we conclude that the effect does not resulted from the free barium cations.

To further verify that the observed effect results from the physical effect of the NPD-water (the induced water structure), and does not result from the differences in the chemical composition (between the NPD-water and the RO water), we performed the following experiments. The nanoparticles were deposited in a passive process, on the plates of the ECD cell with a very low density. The deposition was simply done by placing the NPD-water above the plates for 30 min. In Fig. 7 we show the effect of electrochemical deposition in control solution, but when using the plates with deposited nanoparticles from the NPD-water. Based on AFM scanning we deduced that the density of the deposited particles is lower than about 10 particles per square micrometer. Comparing Fig. 7b to Fig. 6b it is

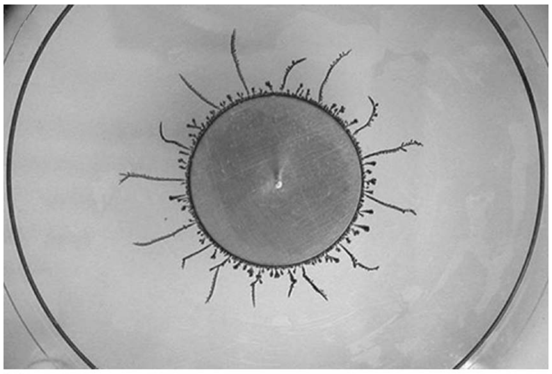
(a)

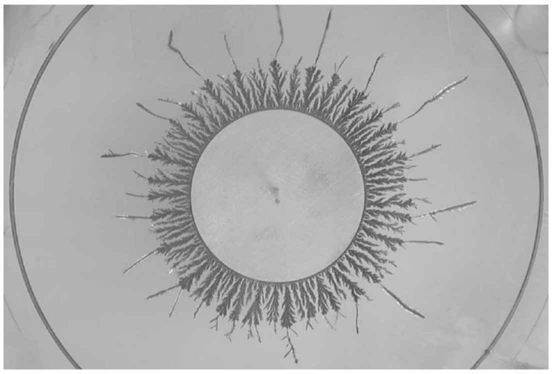
(b)

Figure 7. The effect of nanoparticles deposited on the plates of the ECD cell. The pictures show comparison between (a) the control electrochemical deposition and (b) electrochemical deposition using the same solution as in (a) but performed in the cell after nanoparticles were deposited on the plates. The growth conditions in both cases are for $V = 12.4$ V and $C = 0.2$ M.

evident that the effect of the deposited nanoparticles is similar to that of the doped ones. We note that the plates are rinsed with distilled water after plating to remove residual deposited salts from the NPD-water. These findings hint that the deposited nanoparticles can induce order in the solution presumably due to attraction of nanobubbles. In this regard we note that it is known that nanobubbles tend to accumulate at hydrophobic surfaces.[76] The observed effect of the deposited nanoparticles also provides important support to the idea presented earlier that the selection of the DBM growth is due to the effect of external ordering that competes with the effect of the internal anisotropy of the deposit. We propose that the effect of the deposited nanoparticles is stronger than that of the doped ones (more symmetric and extended DBM patterns), since the network induced by the deposited nanoparticles is more rigid (the particles are anchored to the surface).

The Singular Effect on the Microscopic Scale

According to the new picture of pattern formation,[10-14,42-54] we expect that if the rf-treatment and the nanoparticle doping act as singular perturbations, the observed morphology changes on the macrolevel should go hand-in-hand with significant effects on microscale structure of the deposits. Motivated by these theoretical considerations we performed extensive studies using electron microscopy observations. More specifically, we compared the structure of the DBM and dendritic deposits during growth in control solutions (C), rf-treated solutions (rf), and solutions made from NPD-water (NPD) at different magnifications using SEM. We note that three classes of growth conditions were selected: (1) Low voltages such that the ECD process for (C), (rf), and (NPD) yields DBM patterns on the macroscopic scale; (2) high voltages such that dendritic patterns are observed on the macrolevel for the three types of solutions; (3) intermediate voltage ($V = 12.4$ V) such that for (C) dendrites are observed on the macrolevel and the DBM is exhibited for (rf) and (NPD). In Fig. 8 and 9 we show a comparison between the micrometer scale ordering of the DBM deposits. The results depicted in these figures clearly illustrate significant differences between the microscale structures of the deposits developed in the control solutions vs those developed in the rf-treated solutions and in the solutions made from the NPD-water.

The results show that for these growth parameters the DBM deposit in the control solutions is mainly composed of very wide dendrites while the deposits for both (NPD) and (rf) are composed of narrow branches. The white bulges at the ends of the branches and the dendritic tips are the results of equilibration and oxidation. The patterns shown in these pictures provide a clear illustration that the effects of the rf-treatment and nanoparticle doping are similar and that are both act as a singular perturbation. We note that few nondendritic branches can also be observed in the case of control solutions as can be seen in (c). Yet they have different structures on the smaller level as shown in Fig. 9. At higher voltages the DBM deposits in the control solutions, while the rf-treated solutions and the solutions made from the NPD-water are all mainly composed of dendrites with scattered orientations. There are significant differences in the shape of the dendrites (the tip curvature) and the organization of the side branches. An example of the dendrites embedded in the DBM deposits grown in solutions made from NPD-water are shown in Fig. 11. The dendrites constructing the DBM deposits grown in the rf-treated solutions are similar in shape and organization of the side branches and they both differ from those embedded in the DBM deposits grown in the control solutions. In Fig. 10 we show a comparison between the dendrites developed at high voltage ($V = 13.0$ V) for (C), (NPD), and (rf). The singular effects of the rf-treatment and the nanoparticle doping are reflected in the dramatic changes in the electron microscopy observations. We also show that deposits grown in an rf-treated solution two hours after the treatment have similar structure to that of deposits grown in control solutions. These observations demonstrate that the effect of the rf-treatment does not result from irreversible modifications in the chemical composition of the solutions. Thus the results support our proposed picture that the effects are mediated via physical changes in the water structure induced by the nanobubbles.

The results show the similarity in the microscopic structure between the deposits grown in the rf-treated solution and deposits grown in a solution made from the NPD-water. Both show the existence of additional long-range order in comparison to the deposits grown in the control solutions. We emphasize that the deposits in (b) and (d) are composed of small dendrites (smaller tip curvature) and more ordered side branches than the ones for (rf) and (NPD). These small dendrites are distorted in the pictures here because the smaller tips are subject to faster equilibration during the preparations for the electron microscopy observations. Comparing pictures (a) and (c) we noticed that the effect of the NPD-water is stronger than that of the rf-treatment in the sense that there is more pronounced ordering. Comparing pictures (c) and (d) we note that after a long time (hours) the effect of the rf-treatment fades away as reflected by the fact that the deposit becomes similar to that grown in the nontreated solution. These observations suggest that the effect of the rf-treatment is connected with reversible physical changes—the formation of long range order—and not with irreversible chemical modifications of the rf-treated solutions.

In the previous sections we showed a comparison at the vicinity of the morphology transition between DBM and dendritic patterns on the macrolevel. We presented a plausible explanation to the fact that the DBM morphology is selected at $V = 12.4$ V for (rf) and (NPD) while dendrites are selected (on the macrolevel) in the control solutions. The explanation was based on the idea of competition between the dendritic order emerging from the singular effect of the internal crystalline anisotropy of the deposit and the singular effect of the external water order induced by the nanobubbles. The idea is that, at lower voltages, the effect of the external order dominates the

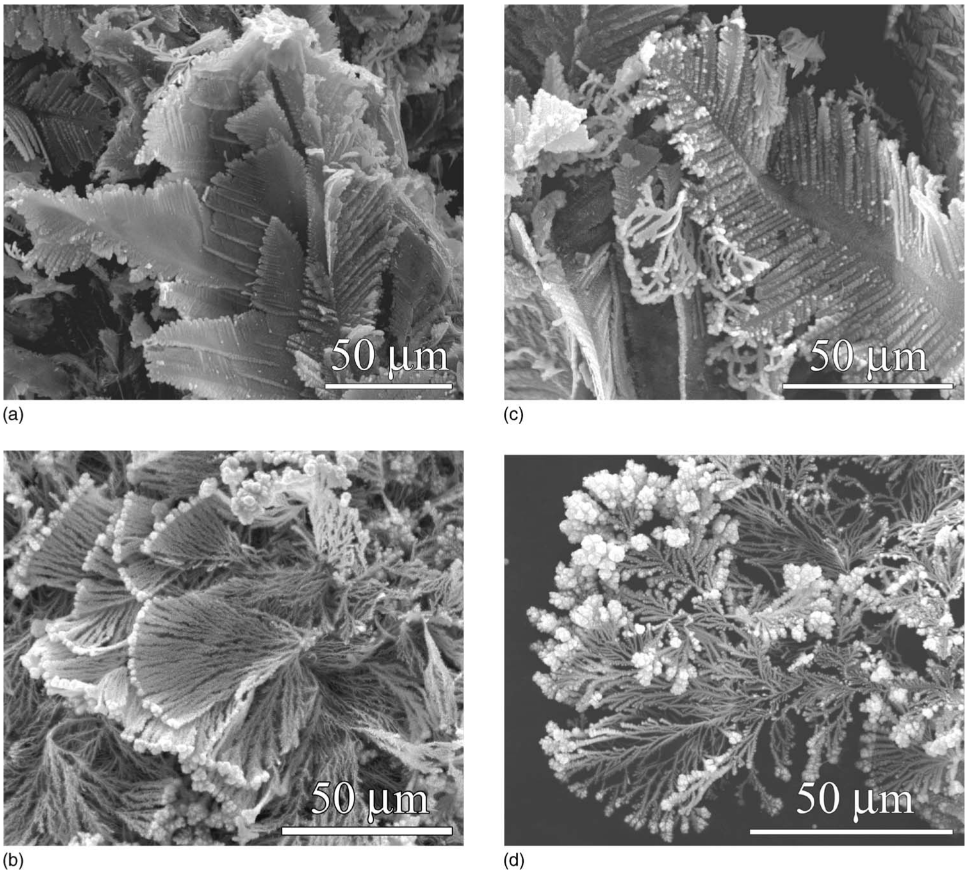

Figure 8. Secondary electron (SE) SEM micrographs of DBM growth on the macrolevel for [(a) and (c)] $V = 8.0$ V and $C = 0.1$ M for (C), (b) (NPD), and (d) (rf).

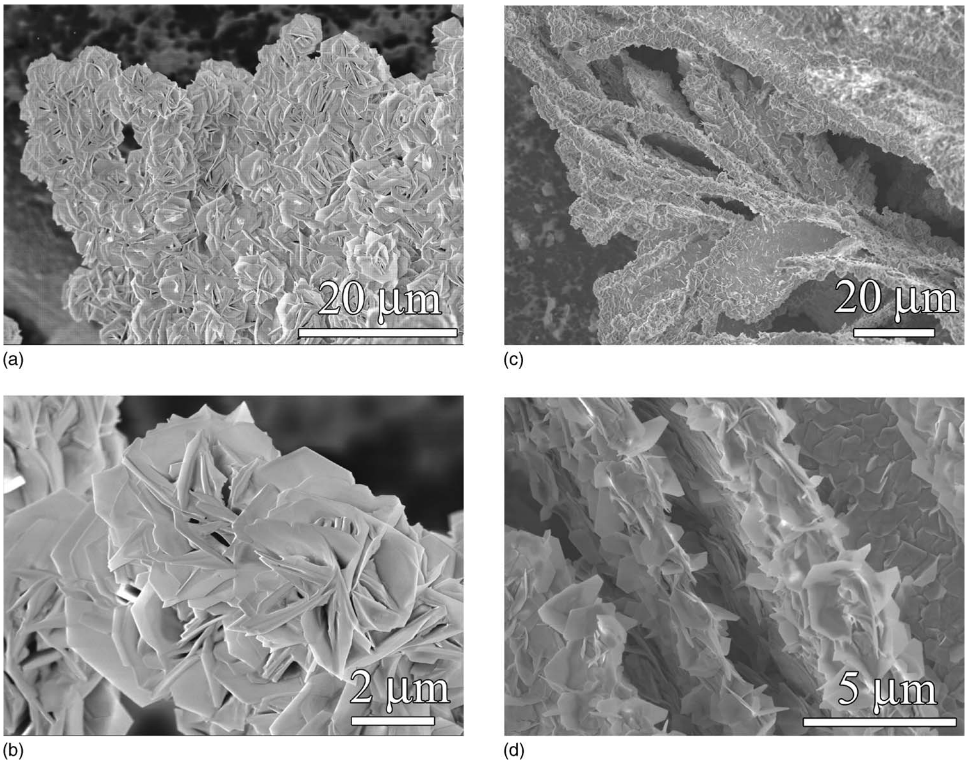

Figure 9. SE SEM micrographs of the DBM deposits for [(a) and (b)] (C) vs [(c) and (d)] (rf). Comparison of the two sets of pictures reveals that additional long range order is induced in the (rf) deposits. Interestingly, this additional ordering goes hand in hand with an apparently less ordered looking structure on the micrometer scale. Growth conditions are $V = 9.0$ V and $C = 0.2$ M.

growth and thus leads to a DBM pattern on the macrolevel. At a higher voltage, since the deposition process is faster, the singular effect of the internal anisotropy is amplified (see Ref. 10-13 and dominates dendritic growth on the macrolevel. We mentioned before that the nanobubbles form a pliable and not rigid network, and hence we expect that the external order will adjust to the developing de-

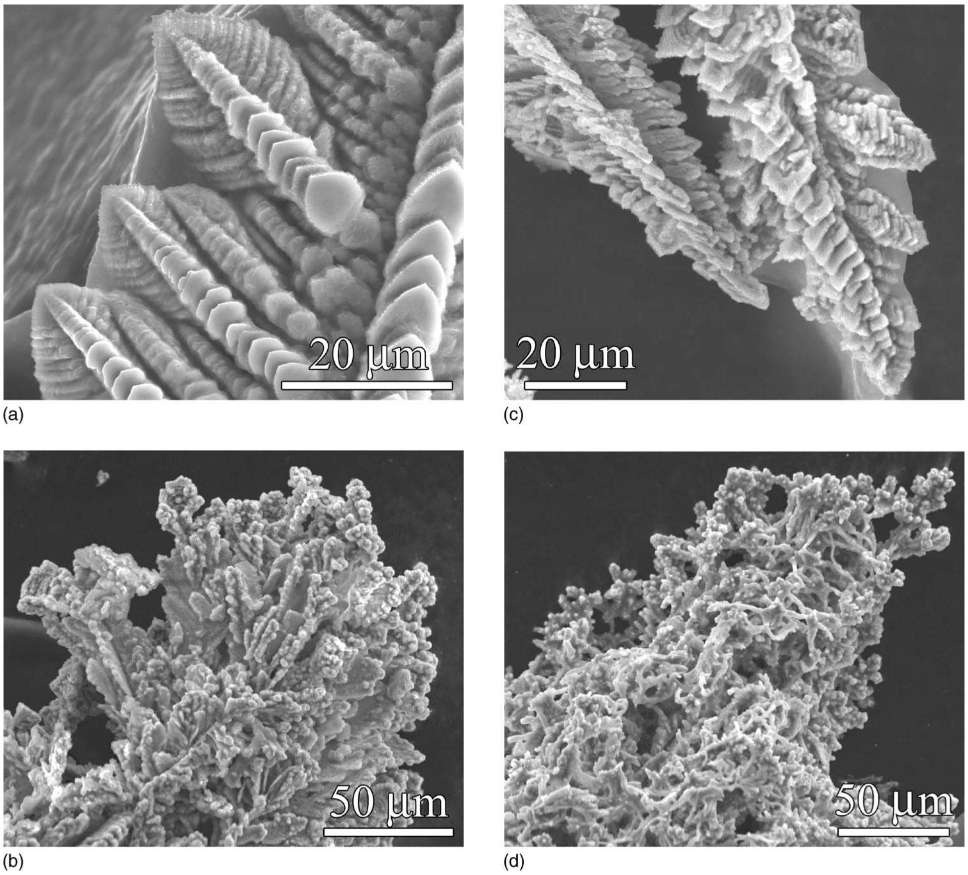

Figure 10. SE SEM micrographs of dendritic growth $V = 13.0$ V and $C = 0.3$ M for (a) (NPD), (b) (C), (c) (rf), and (d) (rf after two hours).

posit but not fade away. Indeed, this is the case as is illustrated in Fig. 11 by comparing the dendritic structure of deposits grown in solutions made from NPD-water at different voltages.

Figure 11 compares between dendritic structures of NPD water at different voltages. In (a) we show the dendrites that compose the deposit at $V = 11.0$ V so that on DBM a pattern is developed on the macrolevel. As is explained in the text at this level of voltage the singular effect of the external order is the more dominant one. In (b) we show the opposite case of growth in high voltage in which the singular effect of the internal anisotropy selects a dendritic pattern on the macrolevel. Yet the singular effect of the external order is reflected in the special ordering of the sidebranches. In (c) and (d) we show the structure of the dendrites embedded in the DBM patterns grown at intermediate voltages, $V = 12.4$ V. In this case, the competition between the internal and external ordering lead to a cascade of order disorder between the different scales. The small dendrites have relatively ordered sidebranches but they have a non-ordered orientation. On a higher magnification, there is a longer range order.

Discussion and Conclusions

The experimental studies presented here were intended to provide additional insight toward a better understanding of a newly observed phenomenon in electrochemical deposition—the singular effect of rf-treatment of the solutions. Using electron microscopy observations, we showed that rf-treatment of an electrolyte solution affects the deposition process and that the effect on the deposit structure spans over all scales, from the microscopic structure, through the micrometer-scale organization, to the macroscopic pattern. To further substantiate the universality of the phenomenon, we also studied electrochemical deposition in solutions where the solvent was nanoparticle-doped water (NPD-water), doped under rf-irradiation as described in the Appendix. We showed that similar and even more pronounced effects were observed with the NPD-water and that the effects could be retained for months after production.

We mentioned in the Introduction that various mechanisms have been shown to act as singular perturbations during electrochemical deposition, including modification of the solution viscosity[19,23,29,30,34,36] and changes in the double layer at the solid-liquid interface[20,24] and in the kinetics of attachment.[22,27,32,34] It is also known, as discussed in the first section, that rf-treatment induces changes in the solution surface tension, in the viscosity, and in the zeta potential. Put together, the above known facts imply, as we explain below, that rf-treatment of an electrolyte solution can, in principle, have singular effects on electrochemical deposition.

The chain of explanation begins with the idea that rf-irradiation of water and aqueous solutions can lead to the formation of stable (hours) gas nanobubbles.[59,60,65,67] The latter induce ordering in the water around them that is assumed to generate the observed anomalous effects of the rf-treatment. This idea is strongly supported by the fact that degassing of the treated water or solutions erases the effects, and rf-treatment has no effect on degassed water.[58-69]

Let us look again at the previously proposed assumptions in the literature regarding the formation and effects of nanobubbles (see the first section): (1) The nanobubbles have long-term stability (hours); (2) the gas-water interface of the nanobubbles is hydrophobic and therefore the water molecules form clathrate shells with an "icelike" structure around the gas nanobubbles; (3) the ordered shells can induce order in the water molecules surrounding the nanobubbles that extends up to a micrometer in range.

Back to electrochemical deposition, the above proposed assumptions provide a plausible explanation to how rf-irradiation can act as a singular perturbation: The water ordering induced around the formed nanobubbles can act as a local (from nano to micro) singular perturbation since it affects the properties of the double layer, the kinetics of attachment, and the diffusion and transport of ions near

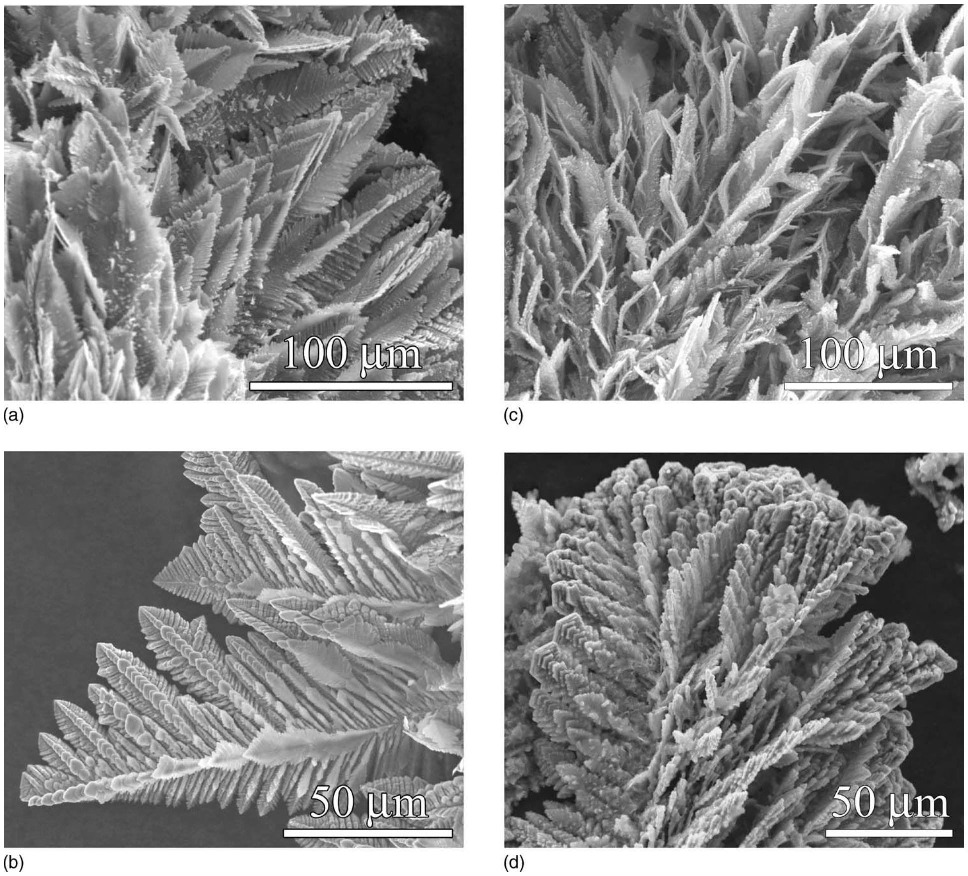

Figure 11. Comparison between the dendritic structures on the microlevel between (NPD) deposits grown at different voltages.

the interface of the deposit. These can explain the observation of micrometer scale structural differences between dendrites grown in the control solution vs those grown in the rf-treated solutions and in the solutions made with the NPD-water.

However, as we pointed out earlier, the additional observations presented here connected with the selection of the DBM morphology for the (rf) and (NPD) might indicate the presence of an additional effect, besides the induced order around the nanobubbles. More specifically, the observations indicate the existence of long-range (dozens of micrometers) ordering that competes with the internal ordering imposed by the crystalline anisotropy of the growing deposit. It was suggested that external long-range order is generated by the nanobubbles that are dispersed in the solution with a nonarbitrary distribution resulting from the collective effect of the exchange interactions between the bubbles. We specifically suggested that the bubble-bubble interactions lead to self-organization of the bubbles into a pliable network with a hierarchical organization of clusters and clusters of clusters of nanobubbles, with larger bubbles being the hubs of the clusters.

We emphasize that this picture also provides a putative explanation to the unexpected effect of the nanoparticle doping—the dramatic stabilization of the rf-treatment anomalous effects. The nanoparticles presumably replace the large gas nanobubbles. Unlike the large gas nanobubbles, the nanoparticles do not expand and hence provide totally stable anchors to the entire array of the gas nanobubbles. Furthermore, we can say that the observation of the stabilization of the effects of rf-treatment by nanoparticle doping supports the idea of hierarchical organization of the nanobubbles. As was pointed out earlier, the idea of the formation of a pliable network of nanobubbles is also consistent with the observed effect of nanoparticles that are deposited on the surfaces of the ECD cell.

Clearly, many additional experiments as well as theoretical investigations need to be performed in order to validate and substantiate the new idea. As a step in this direction, we used isothermal titration calorimetry (ITC) to test the effect of injecting solutions made with the NPD-water into control solutions and vice versa. The preliminary results show an endothermic peak in the former case, implying that the NPD-water solutions have lower free energy, which is consistent with the idea of nonarbitrary distribution. We also note that the magnitude of the effect and the small size of the injected droplets rule out explanations based on chemical activity.

To conclude, we reported here on interesting observations relating to the effects of rf-treatment on electrochemical deposition and its stabilization by nanoparticle doping. We propose that the previously reported anomalous effects of rf-treatment[58-69] together with our new findings hint to the existence of unknown physical phenomena related to the fundamental properties of water. The experiments reported here might provide important clues to revealing these principles.

Acknowledgments

The research reported here has been supported in part by the Tauber Fund and by the Maguy-Glass Chair in Physics of Complex Systems. We are thankful to Do-Coop Technologies, Limited, for providing us with the nanoparticle doped water (Neowater™) and for technical assistance. We specifically thank Amiram Tapiro for his assistance with the sample preparation for the electron microscope observations. Authors Y.K. and L.M. contributed equally to this article.

Tel Aviv University assisted in meeting the publication costs of this article.

Appendix

Nanoparticles Doped Water

As was mentioned in the text, the effects of the rf-treatments can be amplified and stabilized by doping the water with a low density of insoluble nanoparticles. The process is owned by Do-Coop Technologies Ltd. which produces Neowater™. The process starts with reverse osmosis (RO) water that is kept below the anomaly point (i.e., below

4°C) and is irradiated by a rf signal at 915 MHz at a power of 60 W. After 10 min of rf-irradiation, submicrometer size powder of barium titanate that is heated to about 900°C is dropped from the furnace into the water and the rf-irradiation continues for an additional 5 min. Then the water is placed at room temperature for two days, until most of the source powder (that contains larger particles) sinks to the bottom and the clear part of the water is separated.

In Fig. A-1 A we compare the source powder and the nanoparticles at the clear doped water following the production and the separation processes. It can be seen that while the source powder contains large agglomerates composed of small particles with rectangular and faceted shapes, after the doping process most of the particles have almost perfect spherical shape as if due to melting, and their diameter ranges between 10 and 100 nm. These observations indicate that during the production some of the large agglomerates disintegrate and some of the individual particles alter their shape and become spherical. The effect is reminiscent of the phenomena observed during sonochemical synthesise of nanoparticles using cavitation.[96-98] In sonochemistry acoustic signals are used to generate cavitation. We propose that during the production process of the NPD-water, nanobubbles are generated by the rf-treatment and cavitation is generated due to the injection of hot particles into water below the anomaly temperature. The idea is that since the water is kept below the anomaly temperature the hot particles cause local heating that in turn leads to a local reduction of the specific volume of the heated location that in turn causes underpressure in other locations.

The rf-treatment prior to the injection of the particles generates nanobubbles that are used for the cavitation. Interestingly, it takes a long time (hours) for the special properties on the NPD-water to emerge. We propose that during this time the water goes through a self-organization process that includes an exchange of gases with the external atmosphere and selective absorption of the surrounding electromagnetic radiation. We further assume that this self-organization process leads to the formation of the stable structured distribution composed of the nanobubbles and the injected particles that is described in the Discussion section.

In order to estimate the density of the nanoparticles in the NPD-water the water was analyzed using inductively coupled plasma mass spectrometry (ICP-MS) which is a very powerful tool for trace (ppm-ppb) elemental analysis. We found that the NPD-water contains 0.2 mg/L barium and <0.01 mg/L titanium. Since the ratio of the barium vs titanium does not fit the stoichiometric ratio (there is an excess of barium), we assumed that there are free barium ions and titrated the NPD-water with sodium sulfate. As expected, after titration, the barium content decreased to about 0.04 mg/L which is close to the correct stoichiometric ratio of barium titanate. Next, based on the typical size of the nanoparticles as estimated from the electron microscope observations and the measured total amount of titanium (assuming all the titanium is in the nanoparticles), we estimated that the density is below 10^{12} nanoparticles/1 mL. Hence the distance between the nanoparticles is larger than 1mL. For additional investigations of the effect of nanoparticles on water structure, see Ref. 99.

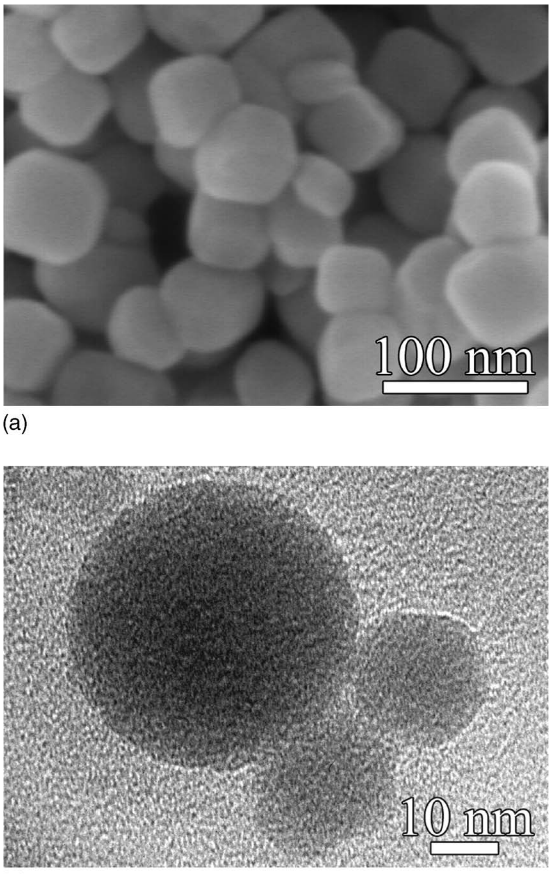

(a)

(b)

Figure A-1. (a) SE SEM micrographs of the source powder and (b) bright field TEM micrographs of the nanoparticles after the injection process.

Back to the free barium ions, it has been shown that there is a spontaneous leaching of barium from barium titanate surfaces of nanoparticles and that the process saturates at pH $\leqslant 7$.[100] With regard to the observed effects in the solution using the NPD-water as a solvent we emphasize that the effects are not due to the chemical activity of the residual barium ions since the concentration is below 1 μM and we used above 0.1 M concentrations of zinc sulfate.

References

1. M. Matsushita, M. Sano, Y. Hayakawa, H. Honjo, and Y. Sawada, *Phys. Rev. Lett.*, **53**, 286 (1984).
2. M. Matsushita, Y. Hayakawa, and Y. Sawada, *Phys. Rev. A*, **32**, 3814 (1985).
3. H. Honjo, S. Ohta, and Y. Sawada, *Phys. Rev. Lett.*, **55**, 841 (1985).
4. Y. Sawada, A. Dougherty, and J. P. Gollub, *Phys. Rev. Lett.*, **56**, 1260 (1986).
5. D. Grier, E. Ben-Jacob, R. Clarke, and L. M. Sander, *Phys. Rev. Lett.*, **56**, 1264 (1986).
6. E. Ben-Jacob, G. Deutscher, P. Garik, N. Goldenfeld, and Y. Lareah, *Phys. Rev. Lett.*, **57**, 1903 (1986).
7. N. Hecker, D. G. Grier, and L. M. Sander, in *Fractal Aspects of Materials*, R. B. Laibowitz, B. B. Mandelbrot, and D. E. Passoja, Editors, Materials Research Society, Pittsburgh, PA (1985).
8. P. Garik, D. Barkey, E. Ben-Jacob, E. Bochner, N. Broxholm, B. Miller, B. Orr, and R. Zamir, *Phys. Rev. Lett.*, **62**, 2703 (1989).
9. Y. Fukunaka, T. Yamamoto, and Y. Kondo, *J. Electrochem. Soc.*, **136**, 3630 (1989).
10. E. Ben-Jacob and P. Garik, *Nature (London)*, **343**, 523 (1990).
11. E. Ben Jacob, *Contemp. Phys.*, **34**, 247 (1993).
12. E. Ben-Jacob and H. Levine, *Nature (London)*, **409**, 985 (2001).
13. E. Ben Jacob, *Philos. Trans. R. Soc. London, Ser. A*, **361**, 1283 (2003).
14. N. Raichman, T. Gabay, Y. Katsir, Y. Shapira, and E. Ben Jacob, in *Continuum Models and Discrete Systems*, D. Bergman and E. Inan, Editors, pp. 187–205, Kluwer Academic Publishers, Dordrecht, The Netherlands (2004).
15. P. Garik, J. Hetrick, B. Orr, D. Barkey, and E. Ben Jacob, *Phys. Rev. Lett.*, **66**, 1606 (1991).
16. D. Barkey, *J. Electrochem. Soc.*, **138**, 2912 (1991).
17. P. P. Trigueros, J. Claret, F. Mas, and F. Sagues, *J. Electroanal. Chem. Interfacial Electrochem.*, **312**, 219 (1991).
18. V. Fleury, M. Rosso, J.-N. Chazalviel, and B. Sapoval, *Phys. Rev. A*, **44**, 6693 (1991).
19. V. Fleury, J.-N. Chazalviel, and M. Rosso, *Phys. Rev. Lett.*, **68**, 2492 (1992).
20. M. Wang and N.-B. Ming, *Phys. Rev. A*, **45**, 2493 (1992).
21. J. M. Riveiro and M. J. Bernal, *J. Non-Cryst. Solids*, **160**, 18 (1993).
22. M. Wang and N.-B. Ming, *Phys. Rev. Lett.*, **71**, 113 (1993).
23. V. Fleury, M. Rosso, and J.-N. Chazalviel, *Phys. Rev. Lett.*, **68**, 2492 (1992); V. Fleury, J.-N. Chazalviel, and M. Rosso, *Phys. Rev. E*, **48**, 1279 (1993).
24. V. Fleury, J. Kaufman, and B. Hibbert, *Phys. Rev. E*, **48**, 3831 (1993).
25. A. Kuhn and F. Argoul, *Fractals*, **1**, 451 (1993).
26. M. Wang, N-B. Ming, and P. Bennema, *Phys. Rev. E*, **48**, 3825 (1993).
27. V. Fleury, J. Kaufman, and B. Hibbert, *Nature (London)*, **367**, 435 (1994).
28. M. Rosso, J.-N. Chazalviel, V. Fleury, and E. Chassaing, *Electrochim. Acta*, **39**, 507 (1994).
29. D. P. Barkey, D. Watt, Z. Liu, and S. Raber, *J. Electrochem. Soc.*, **141**, 1206 (1994).
30. J. Huth, H. Swinney, W. McCormick, A. Kuhn, and F. Argoul, *Phys. Rev. E*, **51**, 3444 (1995).
31. V. Fleury and D. Barkey, *Europhys. Lett.*, **36**, 253 (1996).
32. D. Barkey, F. Obertholtzer, and Q. Wu, *Phys. Rev. Lett.*, **75**, 2980 (1995).
33. V. Fluery, *Nature (London)*, **390**, 145 (1997).
34. G. Marshall and P. Mockos, *Phys. Rev. E*, **59**, 2157 (1999).
35. C. L'eger, J. Elezgaray, and F. Argoul, *Phys. Rev. E*, **61**, 5452 (2000).
36. G. Gonzalez, G. Marshall, F. V. Molina, S. Dengra, and M. Rosso, *J. Electrochem. Soc.*, **148**, 479 (2001).
37. M. Wang, S. Zhong, X-B. Yin, J-M. Zhu, R-W. Peng, Y. Wang, K-Q. Zhang, and N.-B. Ming, *Phys. Rev. Lett.*, **86**, 3827 (2001).
38. S. Bodea, R. Ballou, L. Pontonnier, and P. Molho, *Phys. Rev. B*, **66**, 224104 (2002).
39. S. Wang, K.-Q. Zhang, Q.-Y. Xu, M. Wang, R.-W. Peng, Z. Zhang, and N.-B. Ming, *J. Phys. Soc. Jpn.*, **72**, 1574 (2003).
40. S. Bodea, R. Ballou, and P. Molho, *Phys. Rev. E*, **69**, 021605 (2004).
41. G. Marshall, F. V. Molina, and A. Soba, *Electrochim. Acta*, **50**, 3436 (2005).
42. E. Ben Jacob, P. Garik, T. Muller, and D. Grier, *Phys. Rev. A*, **38**, 1370 (1988).
43. O. Shochet, K. Kassner, E. Ben-Jacob, S. Lipson, and H. Muller-Krumbhaar, *Physica A*, **181**, 136 (1992).
44. O. Shochet, K. Kassner, E. Ben-Jacob, and H. Muller-Krumbhaar, *Physica A*, **187**, 87–111 (1992).
45. O. Sochet and E. Ben-Jacob, in *Computational Crystal Growers Workshop*, J. Taylor, Editor, AMS, Providence (1992).
46. O. Shochet, R. Kupferman, and E. Ben-Jacob, *Growth Patterns in Physical Sciences and Biology*, E. Louis, L. Sander, P. Meaken, and J. M. G. Ruiz, Editors, Plenum, New York (1993).
47. O. Shochet and E. Ben-Jacob, *Phys. Rev. E*, **48**, R4168 (1993).
48. R. Kupferman, O. Shochet, and E. Ben-Jacob, *Phys. Rev. E*, **50**, 1005 (1994).
49. J. L. Hutter and J. Bechhoefer, *Phys. Rev. Lett.*, **79**, 4022 (1997).
50. L. Hutter and J. Bechhoefer, *Phys. Rev. E*, **59**, 4342 (1999).

51. E. Ben Jacob, R. Godbey, N. D. Goldenfeld, J. Koplik, H. Levine, T. Muller, and L. M. Sander, *Phys. Rev. Lett.*, **55**, 1315 (1985).
52. D. A. Kessler, J. Koplik, and H. Levine, *Adv. Phys.*, **37**, 255 (1988).
53. J. S. Langer, *Science*, **243**, 1150 (1989).
54. E. Brener and V. I. Melnikov, *Adv. Phys.*, **40**, 53 (1991).
55. E. Raz, S. G. Lipson, and E. Ben Jacob, *J. Cryst. Growth*, **108**, 637 (1991).
56. M. A. Pasquale, D. P. Barkey, and A. J. Arvia, *J. Electrochem. Soc.*, **152**, 149 (2005).
57. K.-D. Song, K-B. Kim, S.-H. Han, and H. Lee, *Electrochem. Solid-State Lett.*, **7**, 20 (2004).
58. E. Ben Jacob, Y. Aharonov, and Y. Shapira, *Biofilms*, **1**, 239 (2005).
59. M. Colic and D. Morse, *Langmuir*, **14**, 783 (1998).
60. M. Colic and D. Morse, *J. Colloid Interface Sci.*, **200**, 265 (1998).
61. E. Chibowski, S. Gopalakrishnan, M. A. Busch, and K. W. Busch, *J. Colloid Interface Sci.*, **139**, 43 (1990).
62. E. Chibowski, L. Hotysz, and W. Wojcik, *Physicochem. Eng. Aspects*, **92**, 79 (1994).
63. L. Holysz and E. Chibowski, *J. Colloid Interface Sci.*, **165**, 243 (1994).
64. E. Chiboeski and L. Holysz, *Colloids Surf., A*, **101**, 99 (1995).
65. B. G. Yemets, *Int. J. Infrared Millim. Waves*, **21**, 787 (2000).
66. S. Shirata, S. Kabayama, M. Nakano, T. Miura, K. Kusumoto, M. Gotoh, H. Hayashi, K. Otsubo, S. Morisawa, and Y. Katakura, *Biochem. Biophys. Res. Commun.*, **234**, 269 (1997).
67. M. Colic and D. Morse, *Phys. Rev. Lett.*, **80**, 2465 (1998).
68. K. Higashitani, J. Oshitani, and N. Ohmura, *Colloids Surf., A*, **109**, 167 (1996).
69. P. Ball, *Nature (London)*, **423**, 25 (2003).
70. P. Vallée, J. Lafait, L. Legrand, P. Mentré, M.-O. Monod, and Y. Thomas, *Langmuir*, **21**, 2293 (2005).
71. N. F. Bunkin and A. V. Lobeyev, *Phys. Lett. A*, **229**, 327 (1997).
72. N. F. Bunkin, A. V. Kochergin, A. V. Lobeyev, B. W. Ninham, and O. I. Vinogradova, *Colloids Surf., A*, **110**, 207 (1996).
73. L. Belair, *Ann. Phys.*, **27**, 1 (2002).
74. S. Ozeki, J. Miyamoto, J. Ono, S. Wakai, and T. Watanabe, *J. Phys. Chem.*, **100**, 4205 (1996).
75. V. I. Tikhonov and A. A. Volokov, *Science*, **296**, 2363 (2002).
76. P. Attard, *Adv. Colloid Interface Sci.*, **104**, 75 (2003).
77. H.-J. Butt, B. Cappella, and M. Kappl, *Surf. Sci. Rep.*, **59**, 1 (2005).
78. A. C. Simonsen, P. L. Hansen, and B. Klosgen, *J. Colloid Interface Sci.*, **273**, 291 (2004).
79. Z. Xue-Hua, L. Gang, W. Zhi-Hua, Z. Xiao-Dong, and H. Jun, *Langmuir*, **20**, 3813 (2004).
80. X. H. Zhang, N. Maeda, and V. S. J. Caraig, *Langmuir*, **22**, 5025 (2006).
81. J. S. Baker and S. J. Judd, *Water Res.*, **30**, 247 (1996).
82. E. E. Fesenko, and A. Ya. Gluvstein, *FEBS Lett.*, **367**, 53 (1995).
83. E. E. Fesenko, V. I. Geletyuk, V. N. Kazachenko, and N. K. Chemeris, *FEBS Lett.*, **366**, 49 (1995).
84. V. I. Geityuk, V. N. Kazachenko, N. K. Chemeris, and E. E. Fesenko, *FEBS Lett.*, **359**, 85 (1995).
85. H. E. Stanley, S. V. Budyrev, M. Canpolat, M. Meyer, O. Mishima, M. R. Sadr-Lahijany, A. Scala, and F. W. Starr, *Physica A*, **257**, 213 (1998).
86. H. E. Stanley, S. V. Budyrev, M. Canpolat, S. Havlin, O. Mishima, M. R. Sadr-Lahijany, A. Scala, and F. W. Starr, *Physica D*, **133**, 453 (1999).
87. I. Nezbeda and J. Slovác, *Mol. Phys.*, **90**, 353 (1997).
88. P. G. Kusalik and I. M. Svishchev, *Science*, **265**, 1219 (1994).
89. P. M. Wiggins, *Prog. Polym. Sci.*, **20**, 1121 (1995).
90. Q. Liu and J. W. Brady, *J. Am. Chem. Soc.*, **118** 12276 (1996).
91. S. Mashimo, *J. Non-Cryst. Solids*, **172–174**, 1117 (1994).
92. I. M. Svishchev and P. G. Kusalik, *J. Chem. Phys.*, **99**, 3049 (1993).
93. J. R. Grace and D. Harrison, *Chem. Eng. Sci.*, **22**, 1337 (1967).
94. Y. Couder, N. Gerard, and M. Rabaud, *Phys. Rev. A*, **34**, 5175 (1986).
95. M. Rabaud, Y. Couder, and N. Gerard, *Phys. Rev. A*, **37**, 935 (1988).
96. Y. Mizukoshi, T. Fujimoto, Y. Nagata, R. Oshima, and Y. Maeda *J. Phys. Chem. B*, **104**, 6028 (2000).
97. I. U. Abhulimen, X. B. Chen, J. L. Morrison, V. K. Rangari, L. Bergman, and K. Das, *Mater. Res. Soc. Symp. Proc.*, **829**, B2-27 (2004).
98. R. D. West and V. M. Malhotra, *Polym. Eng. Sci.*, **46**, 426 (2006).
99. G. Andrievsky, V. Klochkov, and L. Derevyanchenko, *Fullerenes, Nanotubes, Carbon Nanostruct.*, **13**, 363 (2005).
100. A. Neubrand, R. Linder, and P. Hoffman *J. Am. Ceram. Soc.*, **83**, 860 (2000).